Materials Physics and Mechanics. 2022;50(2): 239-251
Research article
http://dx.doi.org/10.18149/MPM.5022022_5

Submitted: September 16, 2022
Approved: November 9, 2022
Accepted: November 15, 2022

Comparative study of grain fragmentation in iron during cold and warm deformation by uniaxial tension

N.Yu. Zolotorevsky[1,3]✉, V.V. Rybin[1,3], E.A. Ushanova[2,3], A.N. Matvienko[1,3], V.N. Perevezentsev[3]

[1]Peter the Great St. Petersburg Polytechnic University, 29 Politechnicheskaya St., St. Petersburg, 195251, Russia
[2]NRC "Kurchatov Institute" - CRISM "Prometey", 49 Shpalernaya str., St. Petersburg, Russia, 191015
[3]Institute of mechanical engineering problems RAS – branch of the Federal State Budgetary Scientific Institution "Federal Research Center Institute of Applied Physics of the Russian Academy of Science", Belinskogo 85, 603024 Nizhny Novgorod

✉ zolotorevsky@phmf.spbstu.ru

Abstract. The microstructure fragmentation in iron tensile specimens deformed at room temperature and 600°C has been studied by means of EBSD. The aim of the research was to characterize and compare the patterns of fragmentation associated with the appearance and accumulation of deformation-induced high-angle boundaries (HABs). The microstructure was examined on the longitudinal section of necked specimens, in locations corresponding to various true strains from 0.5 to 1.6. It has been shown that a length of deformation-induced boundaries per unit area is characterized by rapid growth at small strains. With further straining, it ceases to grow in a low-angle interval of misorientations, whereas continues to grow in a high-angle interval. The accumulation of HABs occurs considerably faster during cold deformation, mainly through the formation of transition zones between grain-scale deformation bands.
Keywords: iron, plastic deformation, dynamic recrystallization, microstructure, EBSD

Acknowledgements. *The Russian Science Foundation supported this work, project No 21-19-00366.*

Citation: Zolotorevsky NYu, Rybin VV, Ushanova EA, Matvienko AN, Perevezentsev VN. Comparative study of grain fragmentation in iron during cold and warm deformation by uniaxial tension. *Materials Physics and Mechanics*. 2022;52(2): 239-251. DOI: 10.18149/MPM.5022022_5.

1. Introduction

Large plastic deformation of metals leading to their fragmentation [1-3], i.e. the subdivision of initial grains into misoriented fragments, has gained a lot of interest, being a promising approach to obtaining a structural state with extraordinary mechanical properties [4-5]. As a result, a huge number of studies have been carried out in order to characterize ultrafine-grained microstructures produced by various methods of severe plastic deformation [4,6]. At the same time, an initial stage of fragmentation, at which the first deformation-induced high angle boundaries (HABs) appear and start to accumulate, has received much less attention in research.

© N.Yu. Zolotorevsky, V.V. Rybin, E.A. Ushanova, A.N. Matvienko, V.N. Perevezentsev, 2022.
Publisher: Peter the Great St. Petersburg Polytechnic University
This is an open access article under the CC BY-NC 4.0 license (https://creativecommons.org/li-censes/by-nc/4.0/)

According to studies by Rybin and co-workers [1], the first fragment boundaries stand up against previously formed cellular substructure because of their relatively high misorientations and more dense constitution. It has been shown that misorientations of cell boundaries remain at the level of a few degrees, whereas misorientations of the fragment boundaries progressively increase with strain so that HABs are formed eventually [1,7,8]. Given that different lattice rotations of neighboring fragments are caused by different slip systems activity occurring inside them, the fragment boundaries are called geometrically necessary boundaries (GNBs) [9]; these two terms are further used as equivalents. The evolution of misorientation angle distribution both at cell and fragment boundaries has been extensively studied by Hughes and Hansen et al [7,10].

The above results were obtained using transmission electron microscopy (TEM), which has been useful in characterizing dislocation structures, in particular, in distinguishing cell and fragment boundaries by their morphology. However, the nature, and especially the scale, of the fragmentation process are often better suited to the investigation by electron backscatter diffraction (EBSD). The latter method gives a panoramic view of grain-scale heterogeneity, which is very characteristic of the microstructure evolution [11-13], and provides much better statistics than TEM when studying crystallographic parameters of the fragmented structures. During the last two decades, the development of microstructural heterogeneity, including the grain-scale orientation gradients and geometrically necessary dislocations, has been extensively examined using EBSD for strains of not more than ~0.5 [14-18]. Meanwhile, the range of true strains from ~0.5 to 2, where the deformation-induced HABs begin to form, has been far less studied, in particular with respect to the effect of deformation temperature [19,20]. The goal of the present study is to move ahead on this issue. The earlier developed method [21], which allows isolating the contribution of deformation-induced HABs to the overall boundary misorientation distribution, has proven useful in addressing this challenge.

Pure iron deformed by tension has been chosen for the present research. The variation of plastic strain along the neck of the specimens allowed us to study the fragmentation developed in the strain range of interest. We examined the microstructure evolution under conditions of cold and warm deformation, at room temperature and 600°C, respectively. The latter temperature was chosen for the warm deformation taking into consideration that, according to the study by Glover and Sellars [22], notable dynamic recrystallization was observed in α-iron only at temperatures above 600°C. Therefore, when making this choice, we expected to avoid the significant influence of discontinuous recrystallization [23] on the microstructure evolution.

2. Materials and Methods

The material used in this study was a commercially pure iron containing ~0.01% of S and ~0.01% Si in solid solutions as well as particles of manganese sulfides and oxides ranging in size from about 0.1 to 1 μm. The cylindrical specimens were deformed in tension at a strain rate of $5\cdot10^{-4}$ c^{-1} until fracture, at room temperature (using testing machine 2167 P-50) and at 600°C (using universal hydraulic testing machine BiSS, model Nano). The initial diameters of the gauge region of the specimens were 6 mm and 5 mm for deformation at room temperature and 600°C, respectively. Engineering stress-strain curves are shown in Fig. 1. The yield stress is approximately 155 and 76 MPa for room temperature and 600°C, respectively.

The specimens for microstructure examination were cut along the tensile direction (TD), and further, the longitudinal sections were studied. Figure 2 shows these sections represented schematically. Local true strains in the neck of the specimens were estimated from the local diameter D using the equation $\varepsilon = 2log\frac{D_0}{D}$, where D_0 is the initial diameter of the specimen. Finite element modeling showed that the local strain near the specimen axis in the first approximation is equal to the average strain of the given section [24].

EBSD mapping was carried out in a scanning electron microscope LYRA 3 XMN RL using Oxford HKL AZtec™ software, on the equipment of the Centre of Shared Use of Scientific Equipment "Composition, structure and properties of structural and functional materials of NRC "Kurchatov Institute" – CRISM "Prometey". Orientation maps represented in what follows are the inverse pole figure (IPF) maps plotted with respect to TD. The analysis of the maps was performed with the help of MTEX software [25]. The percentage of non-indexed points in the EBSD data presented below was less than 18% for the cold deformation and less than 7% for the warm deformation which enabled the sufficiently reliable reconstruction of the deformation structure. The size of the panoramic maps varied from about 350×350 μm to 150×150 μm, while the scanning step size was reduced from 350 nm down to 200 nm with increasing strain. The examined areas are indicated in Fig. 2 by squares together with corresponding local strains. The statistics associated in what follows with the strain "~1" were obtained by averaging the data from the scans related to strains 0.95 and 1.15, while the ones associated with the strain "~1.5" – from the scans related to strains 1.4 and 1.55.

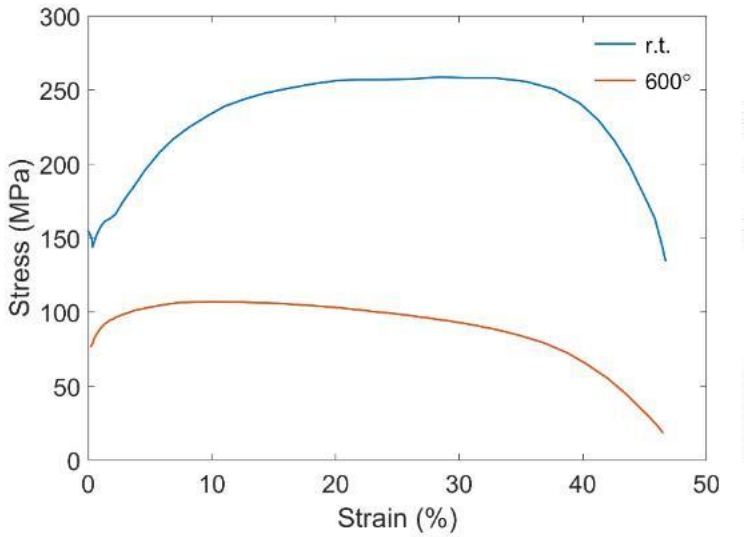

Fig. 1. Engineering stress-strain curves for tensile deformation of iron at room temperature (r.t.) and 600°C. Only plastic strain range is depicted

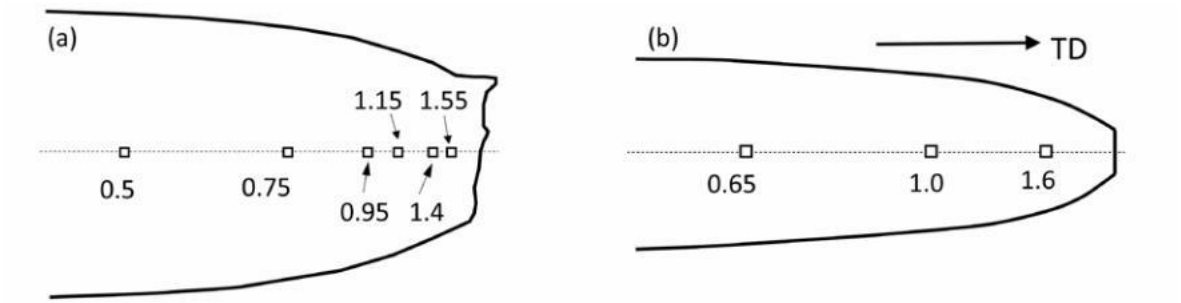

Fig. 2. Schematic drawing of the longitudinal sections of the specimens deformed at room temperature (a) and 600°C (b). Examined regions are depicted by squares, near which local strains are indicated

In order to analyze the evolution of misorientations at deformation-induced boundaries as well as to estimate the fraction of deformation-induced HABs, the earlier proposed method [21] has been used allowing separation of the contribution from the deformation-induced boundaries to the overall misorientation distribution. Its usage is essential for the present

study since it allows assessing the fraction of deformation-induced HABs even when this is of the same order as the fraction of original grain boundaries. The method included the following steps: (i) determination of the misorientation distribution of all boundaries, $l_{tot}(\theta)$, in terms of the boundary length per unit area, (ii) separation of original grain boundaries and determination of their misorientation distribution, $l_0(\theta)$, (iii) obtaining finally the misorientation distribution of DIBs, $l_{DIB}(\theta)$, by subtracting $l_0(\theta)$ from $l_{tot}(\theta)$. This procedure was considered in detail elsewhere [21].

3. Results

Initial microstructure. The as-received condition exhibits nearly equiaxed grains with no deformation substructure inside them (Fig. 3a). The grains are almost randomly oriented (Fig. 3b). An average grain size determined by the linear-intercept method was about 54 μm. Fig. 3a shows that multiple $\Sigma 3$ boundaries (60° around <111> axis) occur in the undeformed iron. From the 60°-peak in the misorientation angle distribution (Fig. 3b), one can conclude that a fraction of such boundaries in the microstructure is about 12%. The morphology of these "twins" differs, however, from the annealing twins observed in FCC metals, which usually appear as flat grain boundaries or intragranular plates. It should be noted that although annealing twins were previously detected in γ-iron, which has been passed slowly through the critical range during cooling, as well as in iron deformed and then recrystallized [26], this phenomenon is still poorly investigated.

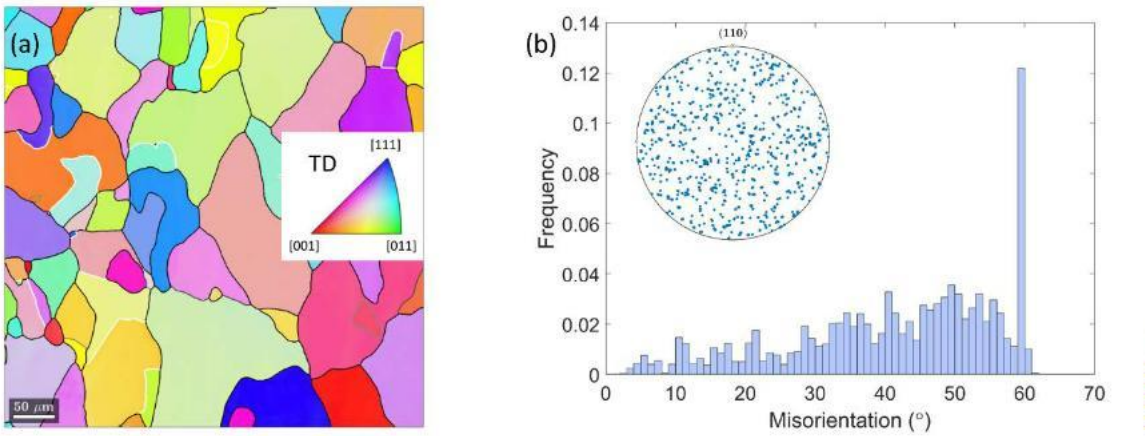

Fig. 3. Typical microstructure of undeformed iron: the inverse pole figure (IPF) map of the microstructure colored with respect to TD (a); the misorientation angle distribution and the texture represented using discrete pole figure (b). Color coding of grain boundaries on the map: random grain boundaries, black; $\Sigma 3$ boundaries, white

General characterization of microstructures evolution. Figures 4a and 4b show typical deformation microstructures developed at room temperature. A pronounced axial <110> texture develops during tension. It is for this reason that IPF maps colored with respect to TD have a rather uniform coloring in spite of highly misoriented microstructure. The original $\Sigma 3$ boundaries present in the initial microstructure are strongly distorted by the plastic deformation, however, some of their segments retain a near-twin misorientation in terms of Brandon criterion, that is, their angular deviation from the ideal $\Sigma 3$ misorientation is smaller than $15°/\sqrt{\Sigma 3} = 8.66°$. At a strain of 0.5, tension leads to a considerable grain-scale orientation heterogeneity (Fig. 4a). With increasing strain, such a heterogeneity manifests itself in the form of deformation bands [23,27-30] separated from each other by zones of high orientation

gradient, often referred to as "transition bands" [27]. Though the latter is usually the locations where low-angle boundaries are concentrated [28], high-angle ones also form there. At a strain of 1.4 (Fig. 4b), the borders between the deformation bands are mostly HABs, and it is not always easy to distinguish them from the original grain boundaries. Some structural peculiarities associated with the formation of HABs as a result of deformation banding will be considered in the next section.

Compared with cold deformation, dynamic recovery has a much greater impact on the microstructure evolution at 600°C (Figs. 4c and 4d). Nevertheless, for a smaller strain, the morphology of the deformation microstructure looks like that observed after cold deformation, in particular, the grain-scale orientation heterogeneity occurs as well, although to a lesser extent (Fig. 4c). New features evidencing dynamic recrystallization appear at strains of = 1 and larger: (i) original grain boundaries develop serrations, and (ii) small new grains form. A region where such grains are concentrated is marked by the rectangle in Fig. 4d.

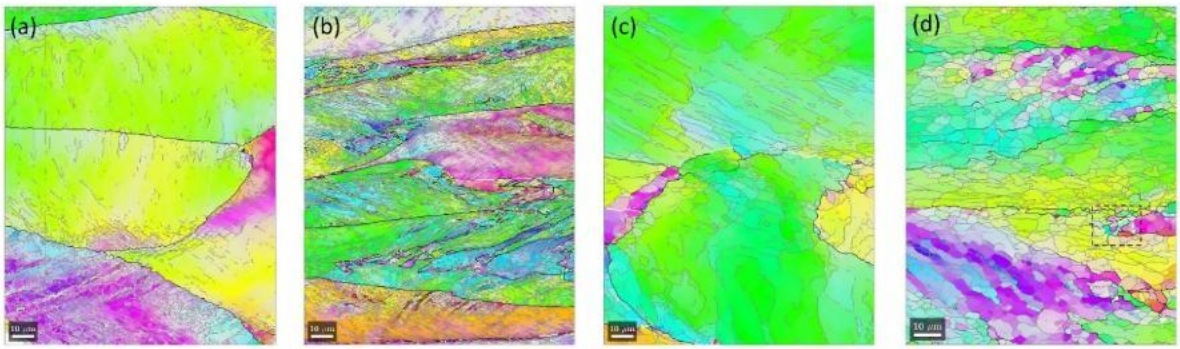

Fig. 4. IPF maps of iron deformed to a strain of 0.5 (a) and 1.4 (b) at room temperature, and to a strain of 0.65 (c) and 1.6 (d) at 600°C. Color-coding of boundaries: 1°< < 45°, grey; > 45°, black; 3 boundaries according to Brandon criterion, white.

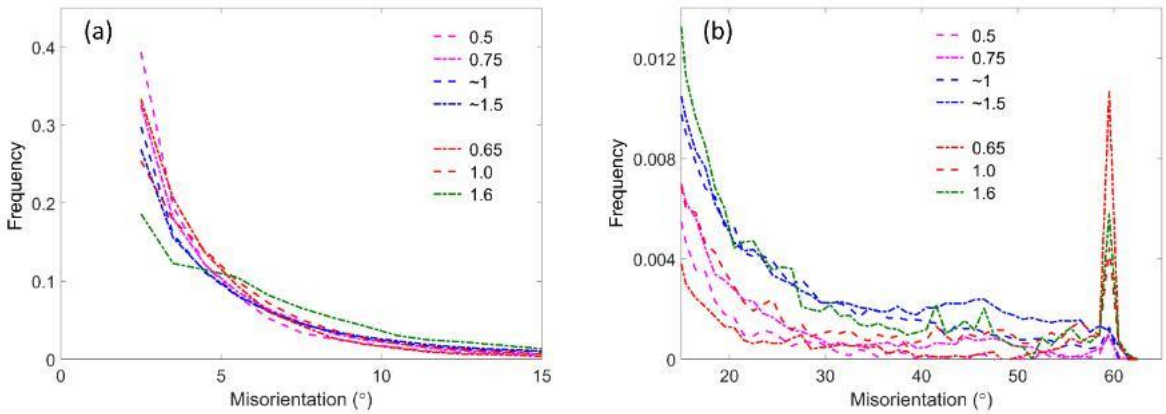

Fig. 5. Effect of strain on misorientation frequency distribution for deformation-induced boundaries in iron deformed by tension at room temperature (blue lines) and 600°C (red lines). True strains are indicated in the legend

The effect of strain on the distribution of misorientations across deformation-induced boundaries is shown in Fig. 5 in the usual way using the frequency $f_{DIB}(\ )$. The latter was calculated here as $l_{DIB}(\ )/L_{DIB}$, where $l_{DIB}(\ )$ is the length of the boundaries having misorientations within the interval (, +1°), and L_{DIB} is the length of all deformation-induced boundaries per unit area. For ease of consideration on one plot, the distributions are shown

using line graphs instead of histograms. Besides, the plot is divided into the low-angle (Fig. 5a) and high-angle parts (Fig. 5b). One can see that the distribution of low-angle boundaries is little dependent on strain, except for the case of warm deformation to = 1.6. At the same time, the relative fraction of HABs increases with strain significantly. The integral characteristic of its growth is shown in Fig. 6.

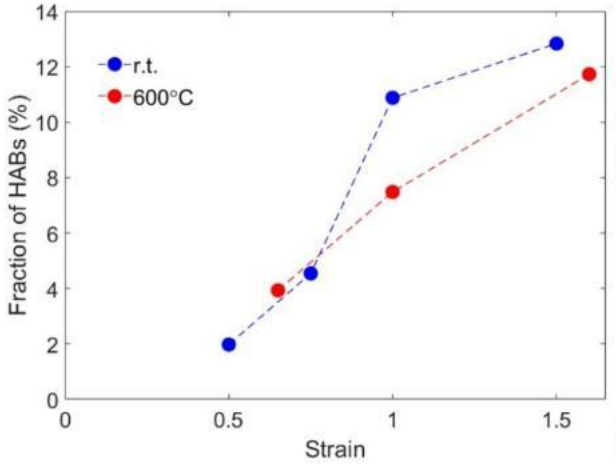

Fig. 6. Effect of strain on the fraction of deformation-induced high-angle boundaries (HABs) in iron deformed by tension at room temperature (r.t.) and 600°C

Figure 7 shows the evolution of misorientation angle distribution represented in terms of the boundary length, $l_{DIB}(\theta)$. This way of presentation allows assessing the total length per unit area ("the specific length") of the boundaries, which fall in a certain angular interval, and not just their relative fraction. One can see that, during cold deformation, $l_{DIB}(\theta)$ increases significantly for all at < 0.75, but with further straining it almost ceases to grow for <15°. Note that the evolution of the cell structure is well known to stagnate at large strains [1,10], however, in the present case, we are looking at GNB rather than cell wall misorientation distribution. Only for the highest angles of disorientation, >40°, $l_{DIB}(\theta)$ continues to grow substantially at all considered strains. Therefore, the gradual increase of fragment misorientations comes to replace the formation of new fragments as the primary mechanism for fragmentation. The broad peak appearing at angles >40° at ~1.5 seems to emerge because mutual lattice rotations of adjacent crystallites exceed the maximal disorientation angle[1] at some boundaries. It is worth noting that, although the relative fraction of deformation-induced HABs reaches only a level of about 12 % (Fig. 6), a ratio of their length to the length of grain boundaries in the initial polycrystalline iron, L_{DIB}/L_0, becomes ~3.5 (Fig. 8).

Though the specific length of the boundaries developed at 600°C is considerably lower than after cold deformation, the shape of misorientation angle distribution remains similar up to a strain of 1 (Fig. 7). It changes qualitatively at = 1.6 owing to a decrease in the specific length of subboundaries with angles < 5°. This occurs, apparently, because of accelerated dynamic recovery that leads to the coarsening of subgrain structure. The specific length of deformation-induced HABs is close to that of original grain boundaries at > 40°. At the same time, a peak appears in the misorientation distribution at 60°. This peak cannot be related to the original 3-boundaries, since corresponding 60°-peak (see Fig. 3b) spreads

[1] The "disorientation" is defined as a minimum angle relationship between crystallites with regard to all 24 cubic symmetry operations. The highest possible disorientation angle varies from 45 to 62.8° depending on the axis of rotation [31].

owing to additional misorientations induced by a strain [32-34]. Hence, its appearance is an indication of some kind of twinning, which takes place during warm deformation.

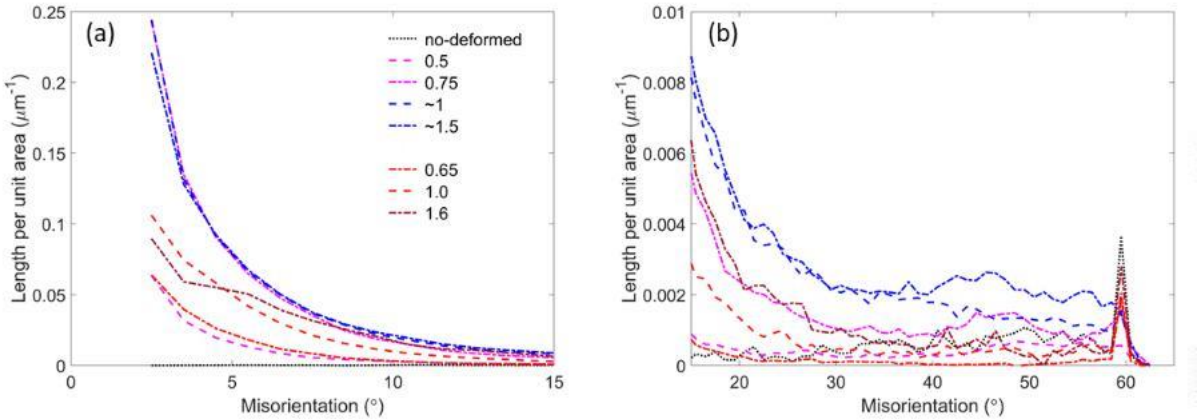

Fig. 7. Effect of strain on misorientation distribution at deformation-induced boundaries represented in terms of boundary length per unit area, in iron deformed by tension at room temperature (blue lines) and 600°C (red lines). The distribution for the initial polycrystalline iron is also presented. True strains are indicated in the legend

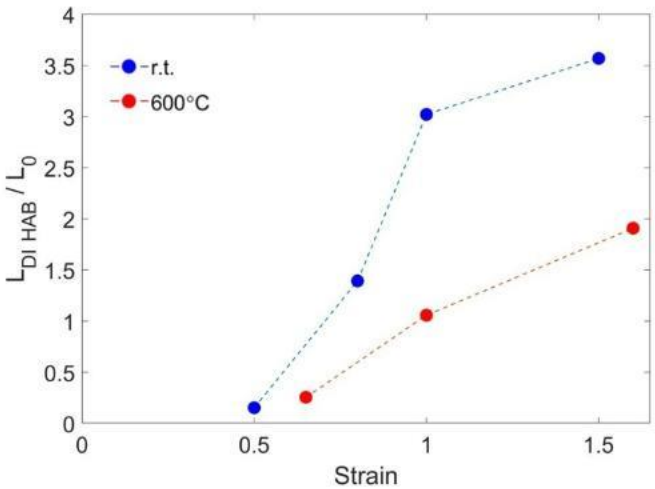

Fig. 8. Effect of strain on the accumulation of HABs in iron deformed by tension at room temperature (r.t.) and 600°C: the ratio of the length of deformation-induced HABs ($L_{DI\,HAB}$) to the length of grain boundaries in the initial polycrystalline iron (L_0)

In general, the accumulation of deformation-induced HABs occurs considerably faster at room temperature than at 600°C in the examined strain range, which is well seen in Fig. 8. In the following sections, the main patterns of HAB formation are considered.

Deformation-induced HABs evolved at room temperature. As noted above, a considerable fraction of HABs is formed within the transition zones developed between the grain-scale deformation bands. It has been shown previously that transition zones of different types occur in tensile strained iron [29,30]. Zones of the first type are similar to ordinary transition bands consisting of low-angle subboundaries, which together provide a high-angle rotation across the band [27]. At the same time, distinct HABs are observed in some parts of such bands. One can suggest that subboundaries appear within the transition band first, and then they merge forming a HAB. In contrast to such narrow transition bands, zones of the second type are wider and more strongly fragmented [30].

Arrays of microbands are also an effective source of deformation-induced HABs in iron according to an assessment made in our earlier work [29]. Unlike so-called microshear bands [8,35], these microbands keep the directionality of the preformed low-angle subboundaries [30], similar to those observed previously in a cold rolled steel [36] or in tantalum alloy [37]. Individual microbands of this type or their small groups can be found in many grains, e.g. Fig. 4b, however, in some grains, such a banding may be the dominant way of in-grain structure evolution. As an example, an array of microbands formed at = 0.75 is shown in Fig. 9a (in order to better reproduce the fine structure of this region, it was mapped with a scanning step of 50 μm). These microbands do not propagate through the whole grain but form a peculiar transition zone between regions of relatively uniform but different orientations ("deformation bands"). It is worth noting that misorientation angles up to ~50° are reached at the boundaries crossed by line scan EF (Fig. 9b), despite the quite small strain.

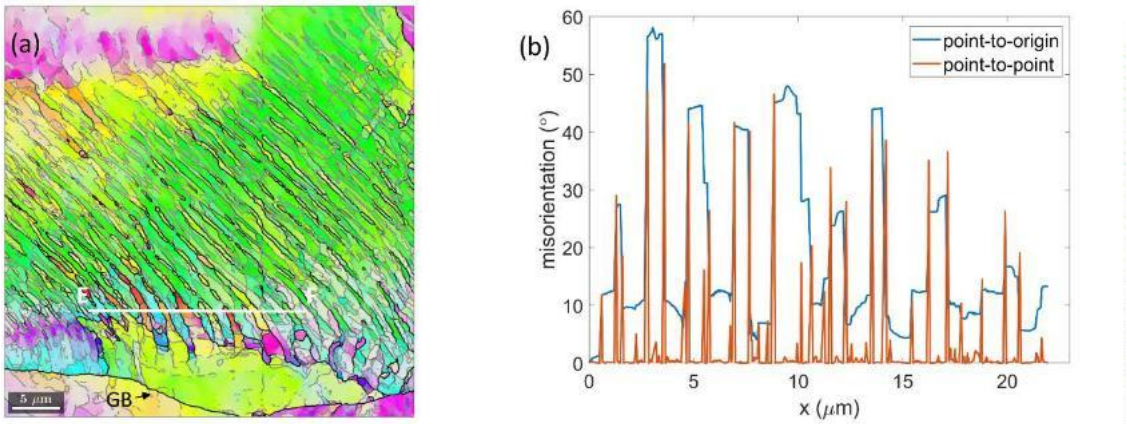

Fig. 9. IPF map of iron deformed at room temperature to a strain of 0.75 (a) and misorientation distribution along segment EF (b). Color-coding of boundaries is the same as in Fig. 4

Deformation-induced HABs evolved at 600°C. Figure 10 shows a region, where characteristic manifestations of dynamic recrystallization take place; some of them are indicated by arrows on the map. The bulging, which is accompanied by the formation of new small grains, is particularly prominent at a grain boundary located on the top of the map (GB1). Such a strong bulging, however, seems to be rare under these deformation conditions. The more usual pattern of nucleation is found at the grain boundary located a little lower (GB2), where a new small grain appears with a limited local migration of the interface. In addition, agglomerations of grains/subgrains with high-angle boundaries form near some original grain boundaries, in particular near grain junctions; one can see an example of such a formation in the lower part of the map in Fig. 10. In these cases, the nucleation of recrystallized grains is rather a result of the evolution of subgrains, namely, the deformation-induced increase in subboundary misorientation. The latter, in its turn, leads to an increase in subboundary mobility and to its local migration [23]. The fundamental fact is that there is no transfer to a long-range growth of new grains: their sizes remain in the order of the neighboring subgrain sizes. Hence, this process may be characterized as continuous dynamic recrystallization [23,38,39].

With increased strain from 1 to 1.6, the character of the microstructure remains the same (Fig. 4), despite the evolution of misorientation distribution (Fig. 7). Namely, the majority of the original grain volume still contains subgrain structure, whereas the sites where new fine grains are concentrated occupy relatively small regions. Such a group of new grains with high-angle boundaries is marked by a rectangle in Fig. 4d. A peak near 60° has been

noted in section 3.1, which remains in the misorientation distribution at all strains. The structural features responsible for this peak can also be found in the area marked in Fig. 4d. They look just like the annealing twins form in the region where dynamic recrystallization occurs. However, these are not plate-like twins specific to dynamic recrystallization of FCC metals [39]. According to Field et al. [40], similar twins were observed during recrystallization when the growth of grains became stagnant. If this mechanism occurs in the present case, the twinning is a manifestation of discontinuous dynamic recrystallization. At the same time, the observation of annealing twins in iron is rather unexpected, so a further study of this phenomenon is necessary.

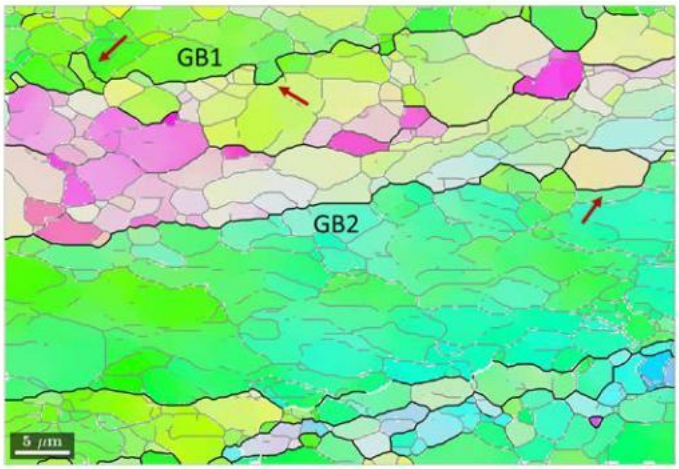

Fig. 10. IPF map of iron deformed at 600°C to strain of 1. Color-coding of boundaries is the same as in Fig. 4

4. Discussion

Despite the significant differences in the patterns of structure evolution, the increase of misorientations at previously formed deformation-induced boundaries is becoming a major mechanism for grain refinement at large strains, both at room temperature and at 600°C. That does not mean, of course, that the formation of new dislocation subboundaries becomes impossible. A dynamic balance seems rather occur between their creation and disappearance. As a result, at the maximum strains studied, the specific length of the lowest-angle subboundaries even decreases: slightly during cold deformation, and significantly during warm deformation. A similar reduction of the low-angle peak, which indicates progress of dynamic recovery, has been frequently observed at sufficiently large strains previously, for example, in steels subjected to cold [41] and warm [20] deformation. Note that the evolution of structure during continuous recrystallization is expected to include the disappearance of some subboundaries [23]. Hence, the recrystallization can also contribute to the reduction of the low-angle peak at 600°C.

As opposed to low-angle boundaries, HABs accumulate steadily with straining, in an approximately linear way for both temperatures (Fig. 8). The fact that the length of deformation-induced boundaries per unit area increases faster at room temperature than at 600°C may be partly associated with the scale, at which the fragmentation process develops. GNBs usually occur at previously formed cell/subgrain boundaries (IDBs) [1,2]. This is likely because the IDBs, despite being penetrable to gliding dislocations [42], can hinder them and thereby contribute to the subdivision of grain into regions, in which different slip systems operate or a different partitioning of the same slip systems occurs [43]. Thus, when cells become smaller with decreasing temperature, a specific length of GNBs is supposed to

increase. At the same time, the main factor is, in our view, the effect of grain-scale deformation banding, which is very pronounced at room temperature, on the formation of HABs. Since different combinations of slip systems operate in neighboring deformation bands from the very beginning of their development, an angle of misorientation between them appears to be on the order of true strain [1,3]. Therefore, at strains of ~1 to 1.5, the deformation banding would have to produce HABs with misorientation angles close to the highest possible disorientation. Indeed, the excess length of the deformation-induced HABs formed at room temperature over the one formed at 600°C is maximal at disorientation angles of ~40° and higher.

5. Conclusions

The process of grain fragmentation in iron subjected to tension at room temperature and 600°C has been studied by means of EBSD analysis. The following conclusions can be drawn from the present investigation.

1. The character of the boundary misorientation distribution remains the same during the early stages of fragmentation, both at room temperature and 600°C. Only after warm deformation up to a strain of 1.6, the shape of the distribution changes considerably owing to the intensification of dynamic recovery and continuous recrystallization.

2. The length of deformation-induced boundaries per unit area ceases to grow with strain in the low-angle range of misorientations, however, it continues to grow in the high-angle range.

3. The relative fraction as well as the length per unit area of deformation-induced HABs increase approximately linearly with strain. The HABs appear and then evolve primarily by way of the gradual increase of misorientations between fragments. The dynamic recrystallization occurring at 600°C gives a relatively small contribution to the grain refinement.

4. Within the examined strain interval, the accumulation of HABs occurs faster at room temperature than at 600°C. This impact of the temperature lowering is mainly due to the more intensive grain-scale deformation banding associated with the formation of transition zones, where HABs are concentrated.

References

1. Rybin VV. *Large plastic deformations and fracture of metals.* Moscow: Metallurgy; 1986. (In Russian)
2. Hansen N, Juul Jensen D. Development of microstructure in FCC metals during cold work. *Phil. Trans. R. Soc. Lond. A*. 1999;357(1756): 1447-1470.
3. Gil Sevillano J, Van Houtte P, Aernoudt E. Large strain work hardening and texture. *Progress in Mater. Sci.* 1980;25(2-4): 69-412.
4. Valiev RZ Langdon TG. Principles of equal-channel angular pressing as a processing tool for grain refinement. *Progress in Mater. Sci.* 2006;51(7): 881-981.
5. Mulyukov RR, Imayev RM, Nazarov AA. Production, properties and application prospects of bulk nanostructured materials. *J. Mater. Sci.* 2008;43: 7257-7263.
6. Estrin Y, Vinogradov A. Extreme grain refinement by severe plastic deformation: A wealth of challenging science. *Acta Mater.* 2013;61(3): 782-817.
7. Hughes DA, Hansen N, High angle boundaries formed by grain subdivision mechanisms. *Acta Mater.* 1997;45(9): 3871-3886.
8. Hurley PJ, Humphreys FJ. The application of EBSD to the study of substructural development in a cold rolled single-phase aluminium alloy. *Acta Mater.* 2003;51(4): 1087-1102.

9. Kuhlmann-Wilsdorf D, Hansen N. Geometrically necessary, incidental and subgrain boundaries. *Scripta Metall. Mater.* 1991;25(7): 1557-1562.
10. Hughes DA, Liu Q, Chrzan DC, Hansen N. Scalling of microsructural parameters: misorientations of deformation induced boundaries. *Acta Mater.* 1997;45(1): 105-112.
11. Delannay L, Mishin OV, Juul Jensen D, Van Houtte P. Quantitative analysis of grain subdivision in cold rolled aluminium. *Acta Mater.* 2001;49(13): 2441-2451.
12. He W, Ma W, Pantleon W. Orientation inhomogeneities within individual grains in cold-rolled aluminium resolved by electron backscatter diffraction. *Mater. Science and Engineering A*. 2008;483-484: 668-671.
13. Hurley PJ, Humphreys FJ. Characterizing the deformed state in Al-0.1Mg alloy using high-resolution electron bacscattered diffraction. *J. Microsc.* 2002;205(3): 218-225.
14. Allain-Bonasso N, Wagner F, Berbenni S, Field DP. A study of the heterogeneity of plastic deformation in IF steel by EBSD. *Mater. Science and Engineering A*. 2012;548: 56-63.
15. Subedi S, Pokharel R, Rollett AD. Orientation gradients in relation to grain boundaries at varying strain level and spatial resolution. *Mater. Science and Engineering A.* 2015;638: 348-356.
16. De Vincentis NS, Roatta A, Bolmaro RE, Signorelli JW. EBSD analysis of orientation gradients developed near grin boundaries. *Materials Research.* 2019;22(1): e20180412.
17. Kundu A, Field DP. Influence of microstructural heterogeneity and plastic strain on geometrically necessary dislocation structure evolution in single-phase and two-phase alloys. *Materials Characterization.* 2020;170: 110690.
18. Liu M, Liu Y, Li H. Deformation mechanism of ferrite in a low carbon Al-killed steel: Slip behavior, grain boundary evolution and GND development. *Mater. Science and Engineering A*. 2022;842: 143093.
19. Humphreys FJ, Bate PS. The microstructures of polycrystalline Al–0.1Mg after hot plane strain compression. *Acta Mater.* 2007;55(16): 5630-5645.
20. Yanushkevich Z, Belyakov A, Kaibyshev R. Microstructural evolution of a 304-type austenitic stainless steel during rolling at temperatures of 773–1273 K. *Acta Mater.* 2015;82: 244-254.
21. Zolotorevsky NY, Rybin VV., Matvienko AN, Ushanova EA, Philippov SA. Misorientation angle distribution of deformation-induced boundaries provided by their EBSD-based separation from original grain boundaries: Case study of copper deformed by compression. *Mater. Characterization*. 2019;147: 184-192.
22. Glover G, Sellars CM, Recovery and recrystallization during high temperature deformation of a-iron. *Metall. Trans.* 1973;4: 765-775.
23. Humphreys FJ, Hatherly M. *Recrystallization and related annealing phenomena, second edition.* Elsevier Science Ltd, Pergamon; 2004.
24. Kuroda M, Uenishi A, Yoshida H, Igarashi A. Ductility of interstitial-free steel under high strain rate tension: Experiments and macroscopic modeling with a physically-based consideration. *International Journal of Solids and Structures.* 2006;43(14-15): 4465-4483.
25. Hielscher R, Silbermann CB, Schmidl E, Ihlemann J. Denoising of crystal orientation maps. *J. Appl. Cryst.* 2019;52: 984-996.
26. Greninger AB. Twinning in alpha iron. *Nature*. 1935;June: 916-917.
27. Dillamore IL, Morris PL, Smith CJE, Hutchinson WB. Transition bands and recrystallization in metals. *Proc. Roy. Soc. A.* 1972;329(1579): 405-420.
28. Kreisler A, Doherty RD. Structure of well-defined deformation bands and formation of recrystallization nuclei in aluminium. *Metal Science.* 1978;12(12): 551-560.

29. Zolotorevsky N, Ushanova E, Rybin V, Perevezentsev V. Characterization of fragmented structure developed during necking of iron tensile specimen. *Letters on Materials.* 2021;11(4): 503-507.
30. Zolotorevsky N, Rybin V, Ushanova E, Ermakova N, Perevezentsev V. Large-scale fragmentation of grains in plastically deformed polycrystalline iron. *Materials Today Communications*. 2022;31: 103816.
31. Gertsman VY, Zhilyaev AP, Pshenichnyuk AI, Valiev RZ. Modelling of grain boundary misorientation spectrum in polycrystals with crystallographic texture. *Acta Metal. Mater.* 1992;40(6): 1433-1441.
32. Rybin VV, Zisman AA, Zolotorevsky NY. Junction disclinations in plastically deformed crystals. *Acta metall. mater.* 1993;41(7): 2211-2217.
33. Cizek P, Whiteman A, Rainforth M. EBSD and TEM investigation of the hot deformation substructure characteristics of a type 316L austenitic stainless steel. *Journal of Microscopy.* 2004;213(3): 285-295.
34. Zolotorevsky NY, Ermakova NY, Sizova VS, Ushanova EA, Rybin VV. Experimental characterization and modeling of misorientations induced by plastic deformation at boundaries of annealing twins in austenitic steel. *J. Mater. Sci.* 2017;52: 4172-4181.
35. Li BL, Godfrey A, Meng QC, Liu Q, Hansen N. Microstructural evolution of IF-steel during cold rolling. *Acta Mater.* 2004;52(4): 1069-1081.
36. Afrin N, Quadir MdZ, Munroe PR, Ferry M, Unusual crystallographic aspects of microband boundaries within {111}<110> oriented grains in a cold rolled interstitial free steel. *ISIJ International.* 2014;54(6): 1346-1352.
37. Ma G, Hughes DA, Godfrey AW, Chen Q, Hansen N, Wu G. Microstructure and strength of a tantalum-tungsten alloy after cold rolling from small to large strains. *J. Mater. Sci. Technol.* 2021;83: 34-48.
38. Sakai T, Belyakov A, Kaibyshev R, Miura H, Jonas JJ. Dynamic and post-dynamic recrystallization under hot, cold and severe plastic deformation conditions. *Progress in Materials Science*. 2014;60: 130-207.
39. Belyakov A, Dudova N, Tikhonova M, Sakai T, Tsuzaki K, Kaibyshev R. Dynamic recrystallization mechanisms operating under different processing conditions. *Materials Science Forum.* 2012;706-709: 2704-2709.
40. Field DP, Bradford LT, Nowell MM, Lillo TM. The role of annealing twins during recrystallization of Cu. *Acta Mater.* 2007;55(12): 4233-4241.
41. Belyakov A, Tsuzaki K, Kimura Y, Regularities of deformation microstructures in ferritic stainless steels during large strain cold working. *ISIJ International.* 2008;48(8): 1071-1079.
42. Gil Sevillano J. Flow stress and work hardening. In: Mughrabi H. (ed.) *Plastic Deformation and Fracture of Materials. Materials Science and Technology, a Comprehensive Treatment*. Weinheim: VCH; 1993. p.19-88.
43. Pantleon W. The evolution of disorientations for several types of boundaries. *Mater. Sci. and Eng. A*. 2001;319-321: 211-215.

THE AUTHORS

Zolotorevsky N.Yu.
e-mail: zolotorevsky@phmf.spbstu.ru
ORCID: 0000-0002-0185-5452

Rybin V.V.
e-mail: rybinvv@mail.com
ORCID: 0000-0003-1619-309X

Ushanova E.A.
e-mail: elinaus@mail.ru
ORCID: 0000-0003-3094-8559

Matvienko A.N.
e-mail: matvienko_an@spbstu.ru
ORCID: 0000-0002-3012-1407

Perevezentsev V.N.
e-mail: v.n.perevezentsev@gmail.com
ORCID: 0000-0002-0437-8540